

On a lattice approach to model flow in cracked concrete

Peter Grassl

Department of Civil Engineering, University of Glasgow, Glasgow, UK
grassl@civil.gla.ac.uk

Submitted to Cement and Concrete Composites, 15th of September 2008

Abstract

This present paper presents a lattice approach to model the influence of cracking on flow in concrete. An earlier mechanical lattice model based on the Voronoi tessellation with a damage-plasticity constitutive model was combined with a new dual lattice of conduit elements for flow analysis. The diffusivity of the conduit elements depends on the crack-opening obtained from the mechanical lattice. The coupled lattice model was applied to three benchmark tests for aligned and random lattices. The results for mechanical loading and flow analysis obtained with the new approach were shown to be independent of the size of lattice elements used.

Keywords: Concrete, cracks, lattice, transport, flow

1 Introduction

Cracking increases the permeability and diffusivity of concrete, which may accelerate the deterioration of concrete structures [30, 12, 27]. Cracks can act, for instance, as pathways for water containing chlorides, which cause corrosion of reinforcement and subsequently may lead to further cracking and spalling of the concrete cover. For cracking induced by mechanical loading, macroscopic crack widths in concrete are a result of complex fracture processes on the meso-scale. For instance, crack bridging and crack tortuosity depend on the material composition and may influence permeability. Other types of loading, such as drying shrinkage subjected to aggregate restraint, lead to distributed micro-cracking, which depends on aggregate size and volume fraction and cannot be uniquely related to a macroscopic crack width [31]. Numerical analysis of the fracture process of concrete on the meso-scale within the framework of the finite element method may increase the understanding of the influence of material composition on micro-cracking and transport properties. However, this requires the development of robust and accurate analysis methods for the interaction of fracture and mass transport.

Modelling of flow in cracked concrete within the finite element framework can be categorised according to nonlinear fracture mechanics approaches. In continuum approaches, fracture is represented as regular fields of localised inelastic strains of finite size by using higher order constitutive laws, such as integral-type nonlocal models [3, 4]. Transport processes in the continuum can be spatially varied according to the amount of accumulated history variables, such as inelastic strains. This approach is

computationally demanding since a fine discretisation is required to be able to describe the localised strain fields. Alternatively, the representation of the fracture process zone is simplified to a displacement discontinuity embedded into the continuum [19, 16, 8]. For these hybrid approaches, localised transport along the discrete crack is coupled with continuum modelling of imbibition into the adjacent material [23, 9, 26, 24]. Coupling of the flow in discrete cracks and the surrounding material creates a bottleneck in these approaches. Finally, in discrete approaches the fracture process is described by the failure of structural elements, such as trusses and beams. Lattice models have shown to be capable of describing complex fracture patterns on the meso-scale of concrete [15, 25, 11]. Furthermore, mass transport can be described by a lattice of conduit elements, which can be linked to the structural lattice to couple fracture and transport processes [10]. Many of these lattice approaches suffer from mesh dependency and fail to describe the continuum response accurately. However, a special type of lattice model for the mechanical response and mass transport was proposed recently, which has been shown to result in mesh-independent and accurate description of the continuum response [6, 7, 5]. In this approach, the cross-sections of structural and transport elements are determined from the Voronoi tessellation. This modelling approach was further developed to describe the interaction of transport along discrete cracks and the surrounding material by introducing an additional lattice of transport elements [20, 28]. This research direction is analogous to the hybrid approaches, with the bottleneck arising in the interaction of the two lattices describing transport along cracks and transport in the adjacent material.

In the present study, a new lattice approach is presented, which is designed to result in a mesh-independent description of the fracture process and mass transport in the cracked material is presented. Transport is modelled by one lattice, which is dual to the lattice used for the mechanical response. The change of transport properties due to localised crack openings are smeared out over the width that is represented by the lattice element, ensuring a mesh-independent description. The first objective of this work was to demonstrate that a lattice dual to the mechanical network accurately represents mass transport in the uncracked continuum. The second objective was to investigate if flow in a cracked media, such as concrete, can be represented independently of the size of the finite element mesh. To the author's knowledge, this is the first lattice approach which models flow in fractured media independently of the mesh size.

2 Combined model for mechanical loading and flow

2.1 Mechanical model

In this work the mechanical response of concrete was described by a lattice approach [18, 6] with a damage-plasticity constitutive model [13]. In the following sections the modelling approach was briefly reviewed.

The lattice model is based on the Voronoi tessellation of the domain. Lattice elements connect nodes, which are the nuclei of the Voronoi polygons (Fig. 2a). The nodes are placed randomly in the domain constrained by a minimum distance d_m . The smaller d_m , the smaller is the size of the lattice elements [6]. Each node has three degrees of freedom, that is two translations and one rotation, which determine the displacement jump at midpoint C of the cross-sections in the local coordinate system as

$$\mathbf{u}_c = \mathbf{B}\mathbf{u}_e \quad (1)$$

where

$$\mathbf{B} = \begin{bmatrix} -1 & 0 & e & 1 & 0 & -e \\ 0 & -1 & -h/2 & 0 & 1 & -h/2 \end{bmatrix} \quad (2)$$

and $\mathbf{u}_e = \{u_1, v_1, \phi_1, u_2, v_2, \phi_2\}^T$. In Eq. (2) e is the eccentricity of the midpoint C and h is the length of the element (Fig. 1b). The cross-sections of the lattice elements are the faces of the Voronoi polygons.

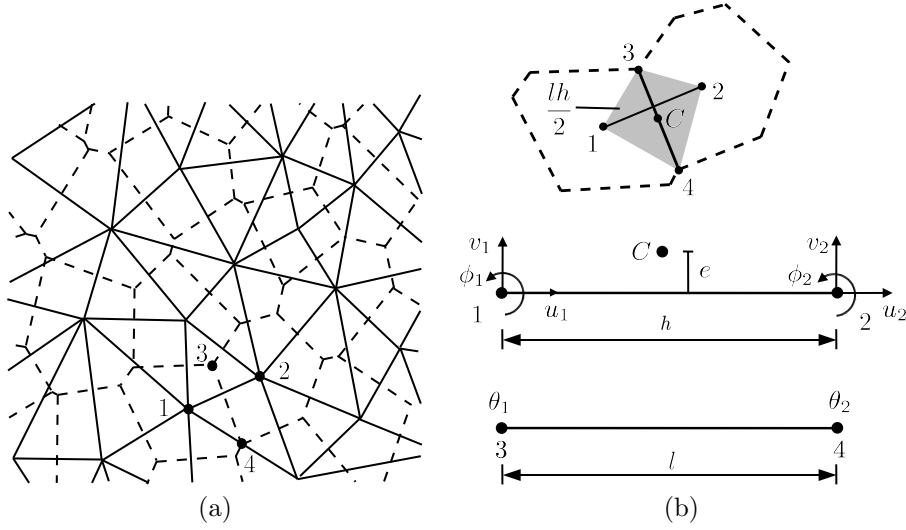


Figure 1: Discretisation: (a) Elements (solid lines) and corresponding cross-sections (dashed lines) of the mechanical lattice obtained from the Delaunay triangulation and dual Voronoi tessellation, respectively. (b) Degrees of freedoms of the lattice elements for the mechanical and transport model in the local Jo-ordinate system.

The element stiffness in the local coordinate system is

$$\mathbf{K}_e = \frac{l}{h} \mathbf{B}^T \mathbf{D} \mathbf{B} \quad (3)$$

where l is the length of the cross-section (polygon facet) and \mathbf{D} is the constitutive stiffness from the constitutive model presented below.

The constitutive model, which relates the strain vector $\boldsymbol{\varepsilon} = \mathbf{u}_c/h$ to the nominal stress vector $\boldsymbol{\sigma}$, is based on a combination of plasticity formulated in the effective stress space and isotropic damage mechanics. The stress-strain law is

$$\boldsymbol{\sigma} = (1 - \omega) \mathbf{D}_e (\boldsymbol{\varepsilon} - \boldsymbol{\varepsilon}_p - \boldsymbol{\varepsilon}_T) = (1 - \omega) \bar{\boldsymbol{\sigma}} \quad (4)$$

where ω is the damage variable, \mathbf{D}_e is the elastic stiffness, $\boldsymbol{\varepsilon}_p = (\varepsilon_{pn}, \varepsilon_{ps})^T$ is the plastic strain, $\boldsymbol{\varepsilon}_T = (\varepsilon_T, 0)^T$ is the eigenstrain, and $\bar{\boldsymbol{\sigma}} = (\bar{\sigma}_n, \bar{\sigma}_s)^T$ is the effective stress. The elastic stiffness is

$$\mathbf{D}_e = \begin{Bmatrix} E & 0 \\ 0 & \gamma E \end{Bmatrix} \quad (5)$$

where E and γ are model parameters controlling both the Young's modulus and Poisson's ratio of the material [14]. For plane stress and a lattice of equilateral triangles, Poisson's ratio ν is

$$\nu = \frac{1 - \gamma}{3 + \gamma} \quad (6)$$

The plasticity part of the damage-plasticity model is based on the effective stress and consists of the yield surface, flow rule, evolution law for the hardening parameter, and loading-unloading conditions. The yield surface is elliptic and its initial size and shape is determined by the tensile strength f_t , the shear strength sf_t and the compressive strength cf_t . The evolution of the yield surface during hardening is controlled by the model parameter μ , which is defined as the ratio of permanent and total inelastic displacements. The scalar damage part is chosen so that linear stress inelastic displacement laws for pure

tension and compression are obtained, which are characterised by the fracture energies G_{ft} and G_{fc} . The equivalent crack opening is defined as $\tilde{w}_c = \|\mathbf{w}_c\|$, where

$$\mathbf{w}_c = h (\boldsymbol{\varepsilon}_p + \omega (\boldsymbol{\varepsilon} - \boldsymbol{\varepsilon}_p)) \quad (7)$$

The crack opening vector \mathbf{w}_c is composed of a permanent and reversible part, defined as $\boldsymbol{\varepsilon}_p$ and $\omega (\boldsymbol{\varepsilon} - \boldsymbol{\varepsilon}_p)$, respectively.

The constitutive response of the damage-plasticity model is illustrated by the stress-strain response for fluctuating normal strains for $\mu = 1$ and $\mu = 0$ (Figure 2). The normal strain is increased to point A

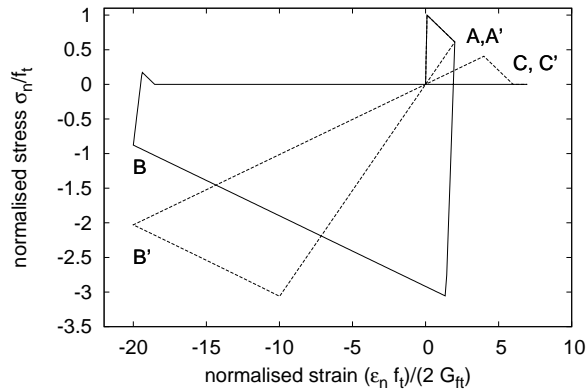


Figure 2: Stress-strain response for fluctuating normal strains for $\mu = 1$ (solid line) and $\mu = 0$ (dashed line).

(A'). Then the strain is reduced to point B (B') and again increased to point C (C'). For $\mu = 0$, a pure damage-mechanics response is obtained and the stress-strain curve is unloaded to the origin. For $\mu = 1$, on the other hand, the combined approach reduces to a pure plasticity model. The unloading is elastic and the compressive strength is reached sooner than for $\mu = 0$. This constitutive model in combination with the present lattice approach results in a meshindependent description of the mechanical response. A detailed description of the components of the model is presented in [13].

2.2 Flow model coupled to the mechanical model

Here, flow was modelled by a new lattice approach, for which the spatial arrangement of the conduit elements is dual to the arrangement of structural elements. The conduit elements are placed along the facets of the Voronoi polygons (Fig. 1a), which determine the positions of cross-sections of the mechanical lattice. Equivalently, cross-sections of conduit elements were positioned on the mechanical lattice elements. The discrete form of the differential equation of the non-stationary flow problem for one conduit element was defined as

$$\mathbf{K}\boldsymbol{\theta} + \mathbf{C}\frac{\partial\boldsymbol{\theta}}{\partial t} = \mathbf{f} \quad (8)$$

where \mathbf{K} and \mathbf{C} are the conductivity and capacity matrix, respectively, t is the time and \mathbf{f} are the external fluxes and the degrees of freedom of the conduit elements are the flow potential $\boldsymbol{\theta} = (\theta_1, \theta_2)^T$ (Fig. 1b) [5]. The conductivity matrix is defined as

$$\mathbf{K} = \frac{h}{l} D \begin{pmatrix} 1 & -1 \\ -1 & 1 \end{pmatrix} \quad (9)$$

where h is the area of the facet crossing the pipe element, l is the length of the pipe element and D is the diffusivity of the material. The capacity matrix \mathbf{C} is

$$\mathbf{C} = \frac{hl}{12} \begin{pmatrix} 2 & 1 \\ 1 & 2 \end{pmatrix} \quad (10)$$

Mechanical loading is assumed to influence the diffusivity of the conduit elements as

$$D = D_0 + \frac{D_c}{h} \quad (11)$$

where D_0 is the initial diffusivity of the undamaged material and D_c is the change of diffusivity due to mechanical loading. The part D_c differs strongly depending on the problem modelled. For moisture transport, for instance, it could be related to the cubic law [30]. In the present study a simple linear law of the form

$$D_c = D_0 \frac{\tilde{w}_c}{w_{\text{fk}}} \quad (12)$$

was chosen, where D_0 is the initial diffusivity of the undamaged material, \tilde{w}_c is the equivalent crack opening from Eq. (7) and w_{fk} is a parameter which controls the slope of the change of diffusivity. The equivalent crack opening is determined in Eq. (7) from the structural lattice element which crosses the conduit element. Since the structural and transport lattices are dual, the cross-section width h of the conduit element is equal to the length of the structural lattice element. An important aspect of the proposed model is the mesh independence, which is achieved by introducing the cross-section h in the expression of the diffusivity in Eq. (11), so that the change of conductivity due to mechanical loading is independent of the width of the conduit elements used. This approach is similar to crack-band approaches, in which the inelastic strain is scaled with respect to the element size to obtain mesh-independent results for strain softening [2, 29]. The parameters D_0 and w_{fk} are material parameters.

3 Results

The modelling approach described above, which was implemented in the object oriented finite element code OOFEM [21, 22], was applied to three benchmark problems. In the first example, a stationary flow field was represented on a random lattice. The second example deals with the coupling of mechanical loading and flow for a lattice, which was aligned to a potential crack path. Finally, mechanical loading and flow was described for splitting due to the expansion of an inclusion with random lattices. The numerical results of the first example were compared to the analytical solution. For the other two examples, possible mesh-dependence of the numerical results were investigated.

3.1 Stationary flow

In the first example, the potential of the new lattice approach to model stationary flow fields was studied. The graded lattice with elements on the facets of Voronoi polygons is shown in Fig. 3. The cross-sections of the conduit elements were chosen in two ways. In the first approach, cross-sections were determined by the dual Delaunay triangulation as described in Section 2.2. In the second approach, a constant cross-section was used, which is the average of the cross-sections obtained from the first approach. The nodes on the left and right hand side of the specimen of length $L = 0.1$ m were subjected to constant potentials of $\theta = 0$ and $\theta = 1$, respectively. For the other two edges, the boundary flux was assumed to be zero ($q_n = 0$). The diffusivity was chosen as $D = D_0 = 1$. The exact solution for this problem is $\theta = x$. The flow along the x -direction for $y = L/2$ for the two approaches is shown in Fig. 4. Additionally, the accuracy of the modelling approach was assessed by comparing the L_2 error norm to the exact solution.

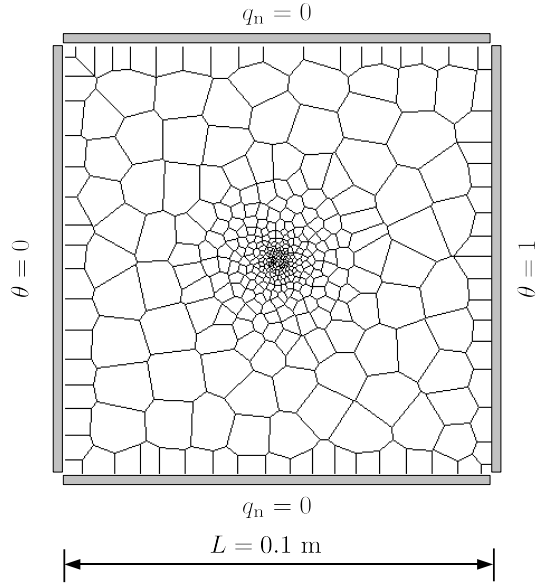


Figure 3: Discretisation of the domain by means of a graded network. Lattice elements were located on the facets of the Voronoi polygons.

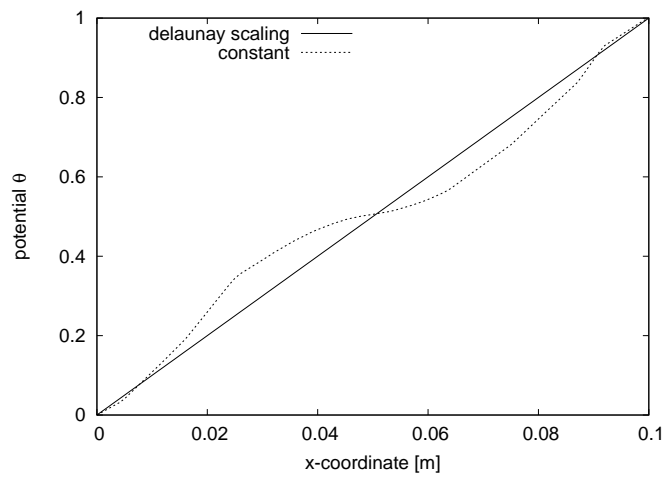


Figure 4: Comparison of the potential θ along the x -direction ($y = L/2$ m) for cross-sections obtained with the Delaunay triangulation and a constant average cross-section.

The error norm is

$$e_r = \frac{\|\theta - \theta^h\|_2}{\|\theta\|_2} \quad (13)$$

where

$$\|\theta - \theta^h\|_2 = \sqrt{\sum_{I=1}^N (\theta(\mathbf{x}_I) - \theta^h(\mathbf{x}_I))^2} \quad (14)$$

and \mathbf{x} is the position of node I , and θ and θ^h are the exact and numerical values of the potential, respectively. The error for constant cross-sections is $e_r = 0.052$, whereas the error for cross-sections obtained from the Delaunay triangulation is $e_r = 5.795 \times 10^{-10}$.

Consequently, the lattice with transport elements placed on the edges of Voronoi tessellation and cross-sections obtained from the dual Delaunay triangulation results in an accurate description of the stationary flow field. The results of the present study complement results obtained from a dual lattice approach, in which the conduit elements are placed on the edges of the Delaunay triangulation and the cross-sections are the facets of the Voronoi tessellation [5].

3.2 Nonstationary flow along an aligned crack

The second example deals with the coupling of fracture and nonstationary flow for an aligned lattice. The analysis is divided into two steps. In the first step, a square specimen of length $L = 0.1$ m was subjected to an eccentrically applied tensile force F . The eccentricity was chosen as $L/4$ (Fig. 5a). The parameters for the mechanical model were set to $E = 40$ GPa, $\gamma = 0.33$, $f_t = 4$ MPa, $G_{ft} = 100$ N/m, $q = 2$, $c = 10$, $G_{fc} = 50000$ N/m, $\mu = 0.001$. The material parameters result in a mechanical response, which is typical for concrete. Three mechanical lattices with minimum distances of $d_{\min} = 0.008$, 0.004 and 0.002 mm were chosen, with the medium mesh shown in Fig. 5a. The mesh was aligned in the middle of the specimen, so that the lattice elements were perpendicular to the crack path. This allows one to evaluate the flow potential along the crack. The result in the form of the load F versus the displacement d at the loading point is shown in Fig. 6a for three lattices. The load-displacement curves are almost completely independent of the size of the lattice elements. At a displacement of $d = 0.1$ m (marked in Fig. 6 by an open circle), the crack almost reaches the right side of the specimen. For this stage, nonstationary flow analyses were performed for three lattices dual to the ones used for the mechanical analyses. The lattice with the medium element size is shown in Fig. 5b. The nodes on the left hand side of the specimen were subjected to $\theta = 1$ at all times, whereas the other nodes have an initial potential of $\theta = 0$ at $t = 0$. The diffusivity D was chosen according to Eq. (12) with $D_0 = 1$ and $w_{fk} = 0.25$ mm. The results are presented by means of the potential θ in x -direction along the crack path ($y = 0.05$ m) in Fig. 7 and the potential θ in y -direction perpendicular to the crack at $x = 0.05$ m in Fig. 8. Five time steps of $t = 0.0001$, 0.0005 , 0.001 , 0.0015 and 0.002 s are presented. The potential along the crack is almost independent of the mesh-size, which is achieved by the special definition of D_{cr} in Eq. (11). The results for the three meshes differ only at the right hand side of the specimen, which might be due to the proximity to the boundary at which the Voronoi tessellation is constrained. Perpendicular to the crack, the potential has its maximum at the crack and decreases away from the crack (Fig. 8). This imbibition process is described independently of the mesh size.

3.3 Fracture and flow in a random mesh

The last example deals with crack propagation and flow in a random mesh. In the previous example the elements in the middle of the specimen were aligned along the crack path, which was useful to evaluate the potential along and perpendicular to the crack. However, lattices for the analysis of fracture processes are usually random, since regular arrangements of lattice elements influence the direction of

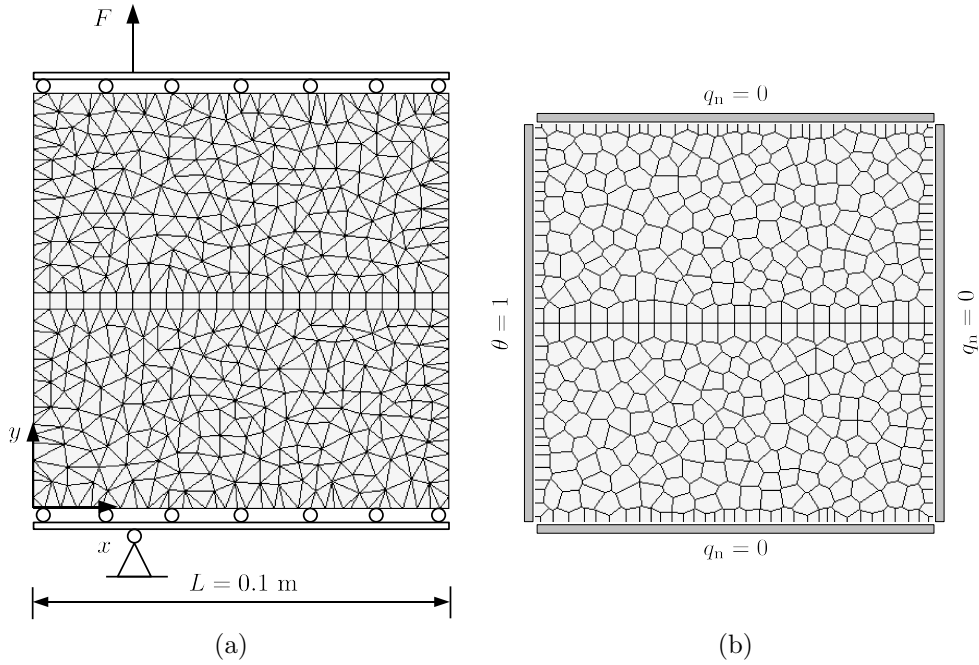


Figure 5: Meshes and loading set-up for (a) structural and (b) transport analysis for the coarse lattice with elements aligned along the potential crack path.

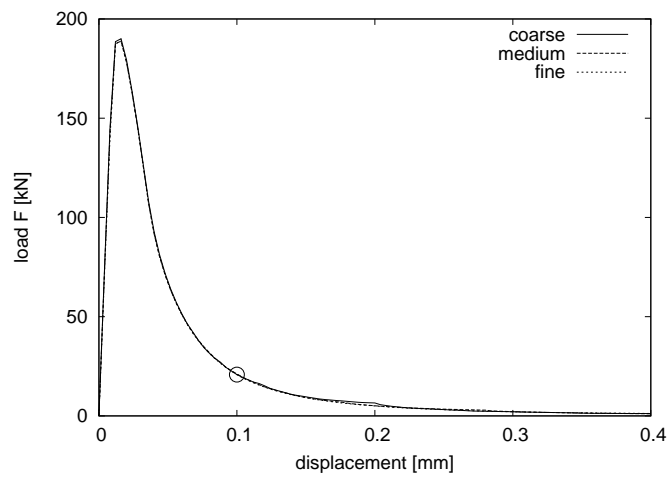


Figure 6: Results of the structural analysis: Load-displacement curves for three element sizes. The open circle marks the stage for which the flow analysis is performed in the second stage of the analysis.

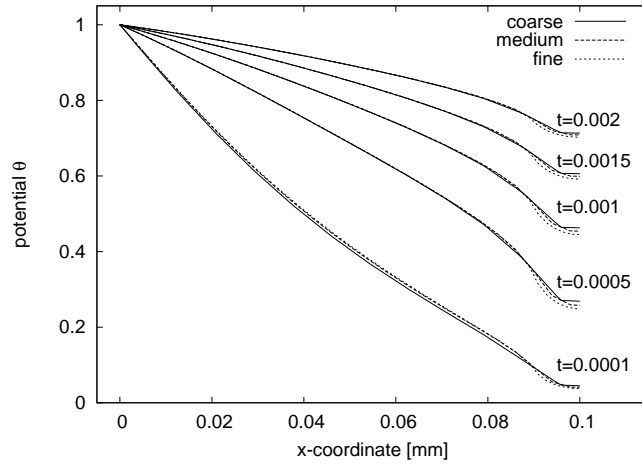


Figure 7: Potential in x -direction along the crack at $y = 0.05$ m for $t = 0.0001, 0.0005, 0.001, 0.0015$ and 0.002 s.

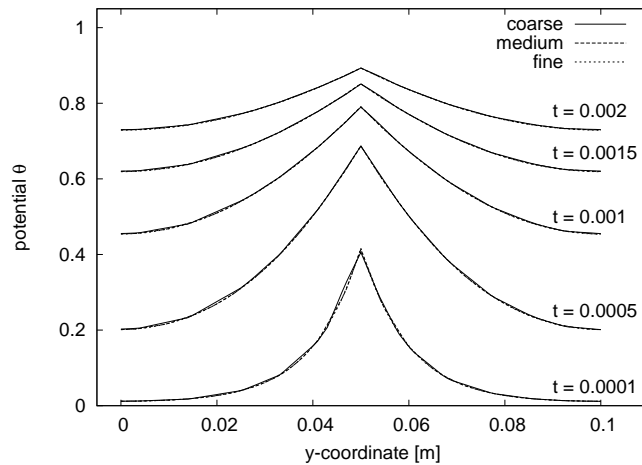


Figure 8: Potential in y -direction perpendicular to the crack at $x = 0.05$ m for $t = 0.0001, 0.0005, 0.001, 0.0015$ and 0.002 s.

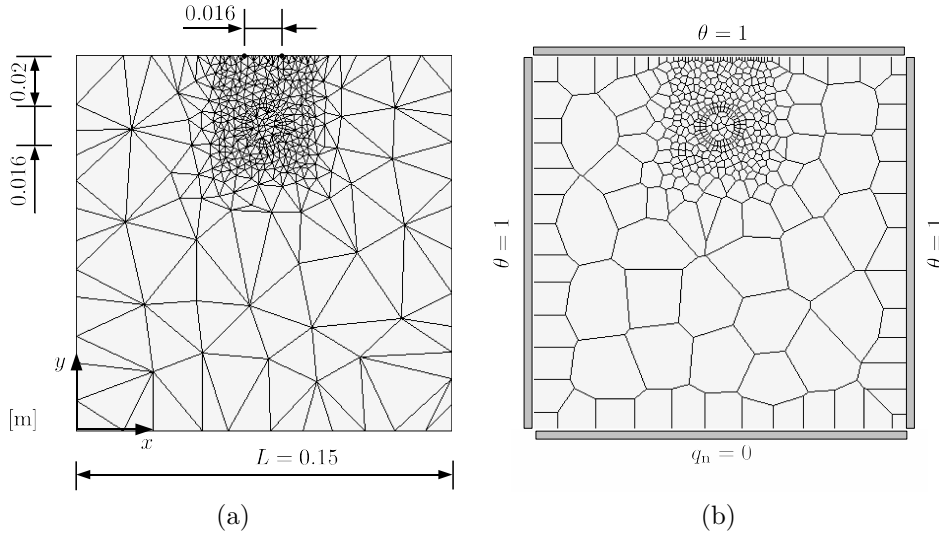


Figure 9: Random lattices with inclusions for (a) structural (b) transport analysis for $d_m = 0.002$ m in the refined regions of the specimens.

crack propagation [17]. In the present example, the mechanical lattice model is used to analyse splitting cracks due to expansion of an inclusion for three random meshes with varying element sizes. The specimen geometry and loading setup was chosen according to corrosion experiments in [1]. The coarse mesh for structural analysis is shown in Fig. 9a. Within the square specimen of length $L = 0.15$ m, an inclusion of diameter $d_a = 16$ mm is located with its center at $x = 0.075$ m and $y = 0.012$ m. The expansion of the inclusion is described by eigendisplacement u_T subjected to elements, which cross the boundary of the inclusion. In these elements the normal component of the eigenstrain in Eq. (4) is $\varepsilon_T = u_T/h$. Thus, the eigenstrain depends on the lattice element size, whereas the displacement is independent. A displacement of $u_T = 0.0665$ mm at these elements is applied incrementally. The crack opening was evaluated at the top of the specimen over a length of $l_c = 0.016$ m (Fig. 9a). The same parameters were used for the mechanical constitutive model as for the previous example. In the refined area, the three lattices were generated with $d_m = 0.002, 0.001$ and 0.0005 m. The results are presented in the form of inclusion expansion u_T versus the crack opening in Figure 10. The initial part of the expansion-crack opening curve is nearly mesh-independent. In a later stage, the results for the three meshes differ. However, the difference is not only due the element size, since the medium mesh overestimates the crack opening obtained from the fine and coarse mesh. Instead, the difference might be largely due to the use of a random arrangement of lattice elements.

In the second step of this example, a flow analysis was performed. The nodes at the top, left and right boundaries were subjected to a constant potential of $\theta = 1$. All other nodes within the specimen had an initial value of $\theta = 0$. The diffusivity D was determined according to Eq. (11). The results of the potential along the x -direction for $y = 0.135$ m is shown in Figure 11 for $t = 0.00001$ s. Similarly, as in the second example, the potential has its maximum at the location of the crack, which is not positioned at the same x -coordinate since the random lattices are used. Nevertheless, the shape and magnitude of the potentials along this section of the specimen are independent of the element size.

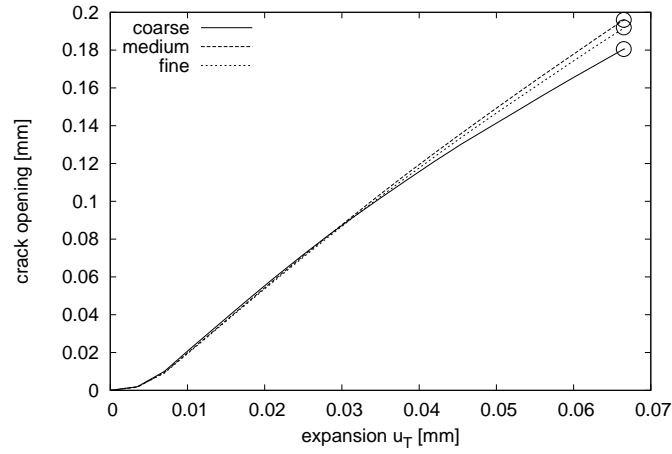


Figure 10: Results of the structural analysis: Crack opening versus eigendisplacement u_T for three mesh sizes. The open circles mark stages at which the flow analysis is performed.

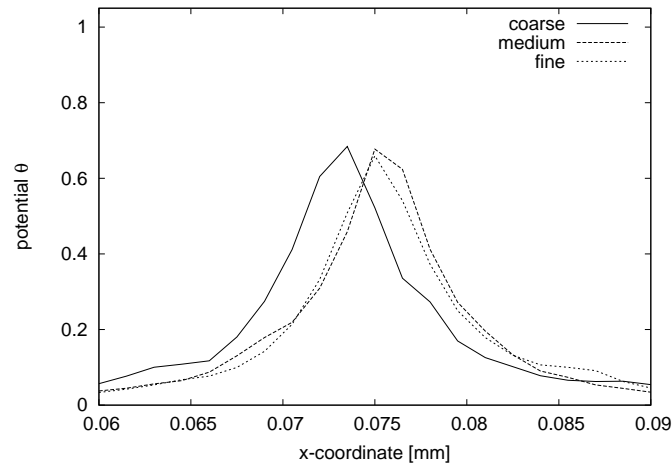


Figure 11: Results of the flow analysis: Potential θ along the x -direction ($y = 0.135$ m) in the refined region of the mesh for three element sizes at a eigendisplacement of $u_T = 0.0665$ mm.

4 Conclusions

In the present work, a lattice approach based on the Voronoi tessellation is presented, which couples mechanical loading to flow analysis by relating the diffusivity of conduit elements to the equivalent crack opening of mechanical lattice elements. The work resulted in the following conclusions:

- The lattice of conduit elements with cross-sections obtained from the Delaunay triangulation results in an accurate description of stationary flow fields for uncracked materials.
- The lattice approach, which couples mechanical loading with flow analysis, results in a mesh independent description of load-displacement curves and flow fields for lattices aligned to the cracks. Mesh-dependence at the specimen boundary is visible, where the Voronoi tessellation is constrained.
- For random lattices, the position of cracks depend on the arrangement of lattice elements. However, the crack openings obtained are independent of the lattice size. Furthermore, flow fields for the cracked material can be described mesh-independently.

The present lattice model is capable of describing the coupling of fracture and flow in concrete independent of the element size. The interaction of discrete and continuous flow, which is a bottleneck of hybrid discrete continuum approaches, is circumvented by modelling both flows by means of one lattice element, in which the discrete flow is smeared out over the width of the elements. Future work deals with the extension of the lattice approach to 3D and its application to the modelling of corrosion induced deterioration.

References

- [1] C. Andrade, C. Alonso, and F.J. Molina. Cover cracking as a function of bar corrosion: Part I-experimental test. *Materials and Structures*, 26(8):453–464, 1993.
- [2] Z. P. Bažant and B.-H. Oh. Crack band theory for fracture of concrete. *Materials and Structures*, 16:155–177, 1983.
- [3] Z. P. Bažant and G. Pijaudier-Cabot. Nonlocal continuum damage, localization instability and convergence. *Journal of Applied Mechanics, ASME*, 55:287–293, 1988.
- [4] Z.P. Bažant and M. Jirásek. Nonlocal Integral Formulations of Plasticity and Damage: Survey of Progress. *Journal of Engineering Mechanics*, 128:1119, 2002.
- [5] J. E. Bolander and S. Berton. Simulation of shrinkage induced cracking in cement composite overlays. *Cement and Concrete Composites*, 26:861–871, 2004.
- [6] J. E. Bolander and S. Saito. Fracture analysis using spring networks with random geometry. *Engineering Fracture Mechanics*, 61:569–591, 1998.
- [7] J. E. Bolander and N. Sukumar. Irregular lattice model for quasistatic crack propagation. *Physical Review B*, 71, 2005.
- [8] G. T. Camacho and M. Ortiz. Computational modelling of impact damage in brittle materials. *International Journal of Solids and Structures*, 33:2899–2938, 1996.
- [9] J. Carmeliet, JF Delerue, K. Vandersteent, and S. Roels. Three-dimensional liquid transport in concrete cracks. *International Journal for Numerical and Analytical Methods in Geomechanics*, 28(78):671–687, 2004.

- [10] G. Chatzigeorgiou, V. Picandet, A. Khelidj, and G. Pijaudier-Cabot. Coupling between progressive damage and permeability of concrete: analysis with a discrete model. *International Journal for Numerical and Analytical Methods in Geomechanics*, 29(10):1005–1018, 2005.
- [11] A. Delaplace, G. Pijaudier-Cabot, and S. Roux. Progressive damage in discrete models and consequences on continuum modelling. *Journal of the Mechanics and Physics of Solids*, 44(1):99–136, 1996.
- [12] B. Gérard, D. Breysse, A. Ammouche, O. Houdusse, and O. Didry. Cracking and permeability of concrete under tension. *Materials and Structures*, 29(3):141–151, 1996.
- [13] P. Grassl and R. Rempling. A damage-plasticity interface approach to the meso-scale modelling of concrete subjected to cyclic compressive loading. *Engineering Fracture Mechanics*, 75:4804–4818, 2008.
- [14] D. V. Griffiths and G. G. W. Mustoe. Modelling of elastic continua using a grillage of structural elements based on discrete element concepts. *International Journal for Numerical Methods in Engineering*, 50:1759–1775, 2001.
- [15] H.J. Herrmann, A. Hansen, and S. Roux. Fracture of disordered, elastic lattices in two dimensions. *Physical Review B*, 39(1):637–648, 1989.
- [16] M. Jirásek. Comparative study on finite elements with embedded cracks. *Computer Methods in Applied Mechanics and Engineering*, 188:307–330, 2000.
- [17] M. Jirásek and Z. P. Bažant. Particle model for quasibrittle fracture and application to sea ice. *Journal of Engineering Mechanics, ASCE*, 121:1016–1025, 1995.
- [18] T. Kawai. New discrete models and their application to seismic response analysis of structures. *Nuclear Engineering and Design*, 48:207–229, 1978.
- [19] N. Moës and T. Belytschko. Extended finite element method for cohesive crack growth. *Engineering Fracture Mechanics*, 69:813–833, 2002.
- [20] H. Nakamura, W. Srisoros, R. Yashiro, and M. Kunieda. Time-dependent structural analysis considering mass transfer to evaluate deterioration process of rc structures. *Journal of Advanced Concrete Technology*, 4:147–158, 2006.
- [21] B. Patzák. Object oriented finite element modeling. *Acta Polytechnica*, 39:99–113, 1999.
- [22] B. Patzák and Z. Bittnar. Design of object oriented finite element code. *Advances in Engineering Software*, 32:759–767, 2001.
- [23] S. Roels, K. Vandersteen, and J. Carmeliet. Measuring and simulating moisture uptake in a fractured porous medium. *Advances in Water Resources*, 26(3):237–246, 2003.
- [24] S. Roels, P. Moonen, K. De Proft, and J. Carmeliet. A coupled discrete-continuum approach to simulate moisture effects on damage processes in porous materials. *Computer Methods in Applied Mechanics and Engineering*, 195(52):7139–7153, 2006.
- [25] E. Schlangen and J. G. M. van Mier. Simple lattice model for numerical simulation of fracture of concrete materials and structures. *Materials and Structures*, 25:534–542, 1992.
- [26] J. M. Segura and I. Carol. On zero-thickness interface elements for diffusion problems. *International Journal for Numerical and Analytical Methods in Geomechanics*, 28(9):947–962, 2004.
- [27] K. Wang, D.C. Jansen, S.P. Shah, and A.F. Karr. Permeability study of cracked concrete. *Cement and Concrete Research*, 27(3):381–393, 1997.

- [28] L. Wang, M. Soda, and T. Ueda. Simulation of chloride diffusivity for cracked concrete based on rbsm and truss network model. *Journal of Advanced Concrete Technology*, 6(1):143–155, 2008.
- [29] K. Willam, N. Bićanić, and S. Sture. Composite fracture model for strain-softening and localised failure of concrete. In E. Hinton and D. R. J. Owen, editors, *Computational Modelling of Reinforced Concrete Structures*, pages 122–153, Swansea, 1986. Pineridge Press.
- [30] P. A. Witherspoon, J. S. Y. Wang, K. Iawai, and J. E. Galw. Validity of cubic law for fluid flow in a deformable rock fracture. *Water Resour. Res.*, 16(6):1016–1024, 1980.
- [31] H. S. Wong, M. Zobel, N. R. Buenfeld, and R. W. Zimmerman. The influence of the interfacial transition zone and microcracking on the diffusivity, permeability and sorptivity of cement-based materials after drying. *Magazine of Concrete Research*, 2008. In press.